J. Fluid Mech. (1991), *vol.* 223, *pp.* 603–629
Printed in Great Britain

A numerical study of nonlinear energy fluxes due to wave–wave interactions Part 1. Methodology and basic results

By D. RESIO[1] AND W. PERRIE[2]

[1] Department of Oceanography, Florida Institute of Technology, Melbourne, Florida, USA

[2] Physical and Chemical Sciences Scotia–Fundy Region, Department of Fisheries and Oceans, Bedford Institute of Oceanography, Dartmouth, Nova Scotia, Canada

(Received 21 February 1989 and in revised form 17 July 1990)

Nonlinear transfer due to wave–wave interactions was first described by the Boltzmann integrals of Hasselmann (1961) and has been the subject of modelling ever since. We present an economical method to evaluate the complete integral, which uses selected scaling properties and symmetries of the nonlinear energy transfer integrals to construct the integration grid. An important aspect of this integration is the inherent smoothness and stability of the computed nonlinear energy transfer. Energy fluxes associated with the nonlinear energy transfers and their behaviour within the equilibrium range are investigated with respect to high-frequency power law, peak frequency, peakedness, spectral sharpness and angular spreading. We also compute the time evolution of the spectral energy and the nonlinear energy transfers in the absence of energy input by wind or dissipated by wave breaking. The response of nonlinear iterations to perturbations is given and a formulation of relaxation time in the equilibrium range is suggested in terms of total equilibrium range energy and the nonlinear energy fluxes within the equilibrium range.

1. Introduction

The pioneering work of Hasselmann in the early 1960s (Hasselmann 1961, 1963*a*, 1963*b*) established a theoretical framework for estimating the net transfer of energy among different frequency-direction components in a wave spectrum. Unfortunately, the resulting integro-differential equation proved to be cumbersome in terms of its functional structure, necessitating that it be evaluated numerically. Early numerical integrations of this equation required very laborious efforts and were limited by computer systems available in the 1960s. With the Joint North Sea Wave Project (JONSWAP) of Hasselmann *et al.* (1973), in which the pattern of spectral evolution along a fetch was observed to agree at least qualitatively with that predicted by these 'wave–wave' interactions, substantial interest was focused on the accurate numerical solution of this equation.

Longuet-Higgins (1976) and Fox (1976) used a simplified approach to estimate the nonlinear wave–wave energy transfer in the vicinity of the spectral peak. Their results were not completely consistent with the earlier approximate computations of Sell & Hasselmann (1972). Moreover, the determination of essential features such as the central minimum and the transition from positive to negative transfer on the right of the spectral peak was unclear from either work. Subsequent studies by Webb

(1978) and Masada (1980) derived transformed versions of the original integro-differential equation which proved to be more adaptable to stable numerical solutions. The solutions of Webb (1978) and Masada (1980) supported the early computational results of Sell & Hasselmann (1972) and suggested that the narrow-band approximations invoked by Longuet-Higgins (1976) and Fox (1976) were somewhat limited in their applicability. More recently, Hasselmann & Hasselmann (1981) have completed a careful study of the nonlinear transfer. They exploited the symmetry of detailed balance (invariance with respect to permutations of all four wavenumbers of a quadruplet $\boldsymbol{k}_1+\boldsymbol{k}_2=\boldsymbol{k}_3+\boldsymbol{k}_4$). Their computations constitute a standard for evaluation of the nonlinear energy transfer, in terms of the detail and accuracy with which they were performed.

As mentioned previously, the need for a better understanding of the magnitude and structure of nonlinear wave–wave interaction energy transfers gained impetus following JONSWAP. Shortly thereafter, Hasselmann *et al.* (1976) considered the shape-stabilizing effect of wave–wave interactions on wave spectra and concluded that wave–wave interaction effects were so strong that wave spectra were effectively controlled, during periods of active wave generation, by a dynamic balance between wind inputs and the wave–wave interactions. Questions concerning the role of wave–wave interactions in governing spectral shapes have arisen since Hasselmann *et al.*'s (1976) study.

Postulating the stationary distribution corresponding to Kolmogorov's inertial subrange, Kitaigorodskii (1983) showed that energy fluxes due to wave–wave iterations should produce an f^{-4} equilibrium range in the spectrum, rather than the f^{-5} form assumed in the JONSWAP spectrum. This was also the result found by Zakharov & Filonenko (1966), as the exact stationary solution to the wave–wave iteration Boltzmann integral for an isotropic field of weakly nonlinear waves. However, Phillips (1985) suggested that a detailed balance of all source terms, including wind input, wave breaking and wave–wave interactions, could produce an f^{-4} equilibrium range and that knowledge of all source terms was necessary to understand the net scaling involved in establishing an equilibrium range. The numerical study of Komen, Hasselmann & Hasselmann (1984) examined the balances among all source terms in a 'fully developed' sea for frequencies extending from the vicinity of the spectral peak f_{p} and up to 2.5 times f_{p}, basing their nonlinear transfer calculation on Hasselmann & Hasselmann (1981).

Recently, Toba, Okada & Jones (1988) suggested that an energy flux must exist from high frequencies to low frequencies in the equilibrium range, as a result of their investigation of characteristics of the relaxation of a deep water wave spectrum under a decreasing wind. This is in addition to the more widely recognized flux from low frequencies to high frequencies in the Kolmogorov subrange. Therefore, a simple analogue to the one-dimensional cascade of energy in turbulence may not be appropriate for surface gravity waves.

Along with theoretical and conceptual developments related to the role of wave–wave interactions in wave generation and the influence of these interactions on spectral shape, a parallel continuing effort has been devoted to obtaining accurate parameterizations of the complete Boltzmann integral. Barnett (1968), Barnett & Sutherland (1968) and Ewing (1971) based parameterizations of complete integrals on the Neumann spectrum and Pierson–Moskowitz spectrum, respectively. Resio (1981) investigated parameterizations based on the scaling laws for f^{-5} spectra and also inherent in the complete integral. Hasselmann *et al.* (1985) and Hasselmann & Hasselmann (1985) examined approximations using empirical orthogonal functions

and also parameterizations based on the superposition of a small number of discrete interaction configurations. The latter type of approximation has been adopted into the WAM model (Hasselmann *et al.* 1989). Since this model is the subject of considerable international investigation, the adequacy of the parameterization is of interest to most wave modellers.

It appears from the issues raised here that estimation of the effects of nonlinear wave–wave interactions has assumed an important role in wave generation and modelling research. In spite of this, most probably owing to the complexity of the numerical problem, few efforts have been made toward establishing a clearer formulation for some of the fundamental characteristics of the nonlinear energy transfers. The present paper will attempt to remedy this situation, at least in part. We begin by formulating an efficient numerical scheme which should assist in understanding some of the inherent scaling properties of the nonlinear energy transfer. This allows computation of the nonlinear transfer on a very fine integration grid and also achieves high numerical stability. This scheme will then be used to investigate the behaviour of nonlinear energy fluxes with respect to high-frequency power law, peak frequency, peakedness, spectral sharpness and angular spreading. We also consider spectral evolution with respect to time and the response of nonlinear wave–wave interactions to perturbations within the spectrum.

2. Evaluation of the nonlinear flux integral

To date most researchers have concentrated on solution of the 'source function' form for nonlinear wave–wave interactions. In this form, the collision integral for four resonantly interacting waves allows evaluation of the net rate of change of energy (or action) for a given wavenumber within the spectrum. Following Hasselmann (1961) the integral can be written as

$$\frac{\partial n(\boldsymbol{k}_1)}{\partial t} = \iiint \mathscr{C}^2(\boldsymbol{k}_1, \boldsymbol{k}_2, \boldsymbol{k}_3, \boldsymbol{k}_4)\, \mathscr{D}(\boldsymbol{k}_1, \boldsymbol{k}_2, \boldsymbol{k}_3, \boldsymbol{k}_4)$$
$$\delta(\boldsymbol{k}_1+\boldsymbol{k}_2-\boldsymbol{k}_3-\boldsymbol{k}_4)\delta(\omega_1+\omega_2-\omega_3-\omega_4)\,\mathrm{d}\boldsymbol{k}_2\,\mathrm{d}\boldsymbol{k}_3\,\mathrm{d}\boldsymbol{k}_4, \quad (2.1)$$

where $\boldsymbol{k}_i$ is the ith interacting vector wavenumber, ω_i is the radial frequency of the ith wavenumber and $n(\boldsymbol{k}_1)$ is the action density at wavenumber $\boldsymbol{k}_1$. The coupling coefficient $\mathscr{C}^2$, is a complicated function of wavenumbers $\boldsymbol{k}_i$ and frequencies ω_i. The density function $\mathscr{D}$, varies cubically in the spectral densities and may be expressed as

$$\mathscr{D}(\boldsymbol{k}_1, \boldsymbol{k}_2, \boldsymbol{k}_3, \boldsymbol{k}_4) = n(\boldsymbol{k}_1)\, n(\boldsymbol{k}_2)\, n(\boldsymbol{k}_3) + n(\boldsymbol{k}_2)\, n(\boldsymbol{k}_3)\, n(\kappa_4)$$
$$- n(\boldsymbol{k}_1)\, n(\boldsymbol{k}_3)\, n(\boldsymbol{k}_4) - n(\boldsymbol{k}_1)\, n(\boldsymbol{k}_2)\, n(\boldsymbol{k}_4). \quad (2.2)$$

An efficient form for integration is obtained by removing the delta functions from (2.1) through the transformation which results in

$$\frac{\partial n(\boldsymbol{k}_1)}{\partial t} = 2\int T(\boldsymbol{k}_1, \boldsymbol{k}_3)\,\mathrm{d}\boldsymbol{k}_3, \quad (2.3)$$

where

$$T(\boldsymbol{k}_1, \boldsymbol{k}_3) = \oint \mathscr{C}^2 \mathscr{D} \left|\frac{\partial \mathscr{W}}{\partial \boldsymbol{n}}\right| \theta(\boldsymbol{k}_1, \boldsymbol{k}_3, \boldsymbol{k}_4)\,\mathrm{d}\boldsymbol{s} \quad (2.4)$$

is the nonlinear transfer integral, $\mathscr{W} = \omega_1+\omega_2-\omega_3-\omega_4$ and the frequency resonance condition is

$$\mathscr{W} = 0. \tag{2.5}$$

Unit vector $\boldsymbol{s}$ is along the interaction locus, defined in $\boldsymbol{k}_2$-space by the constraint $\mathscr{W} = 0$. Unit vector $\boldsymbol{n}$ is normal to that locus. The wavenumber resonance condition is $\boldsymbol{k}_1+\boldsymbol{k}_2-\boldsymbol{k}_3-\boldsymbol{k}_4 = 0$, and θ may be represented as

$$\theta(\boldsymbol{k}_1, \boldsymbol{k}_3, \boldsymbol{k}_4) = \begin{cases} 1 & \text{when} \quad |\boldsymbol{k}_1-\boldsymbol{k}_3| \leqslant |\boldsymbol{k}_1-\boldsymbol{k}_4| \\ 0 & \text{when} \quad |\boldsymbol{k}_1-\boldsymbol{k}_3| > |\boldsymbol{k}_1-\boldsymbol{k}_4|. \end{cases} \tag{2.6}$$

Webb (1978) showed that this provided a stable, efficient form for integration. However, it was still tedious to apply this formulation since for each different value of $\boldsymbol{k}_1$ and $\boldsymbol{k}_3$, the locus equation had to be solved and at each point along the locus in $\boldsymbol{k}_2$-space, the coupling coefficient, density term, Jacobian term and phase space volume had to be evaluated.

This problem was simplified by Tracy & Resio (1982) using a polar grid in wavenumber space with the radial coordinate spaced according to

$$\boldsymbol{k}_{m+1} = \lambda \boldsymbol{k}_m \tag{2.7}$$

where $m+1$ is the radial index shown in figure 1. It may be demonstrated that for any geometrically similar $\boldsymbol{k}_1$ and $\boldsymbol{k}_3$, for example $|\boldsymbol{k}_1'-\boldsymbol{k}_3'| = \lambda|\boldsymbol{k}_1-\boldsymbol{k}_3|$, the locus equation scales linearly in λ also. Specifically, for each point along the original locus, a geometrically similar point exists in a scaling locus such that $\boldsymbol{k}_2' = \lambda \boldsymbol{k}_2$. From the resonance condition for wavenumbers we obtain $\boldsymbol{k}_4' = \lambda \boldsymbol{k}_4$, and for each combination of four wavenumbers satisfying $(\boldsymbol{k}_1', \boldsymbol{k}_2', \boldsymbol{k}_3', \boldsymbol{k}_4') = \lambda\,(\boldsymbol{k}_1, \boldsymbol{k}_2, \boldsymbol{k}_3, \boldsymbol{k}_4)$ it follows that

$$\mathscr{C}^2(\boldsymbol{k}_1', \boldsymbol{k}_2', \boldsymbol{k}_3', \boldsymbol{k}_4') = \lambda^6 \mathscr{C}^2(\boldsymbol{k}_1, \boldsymbol{k}_2, \boldsymbol{k}_3, \boldsymbol{k}_4), \tag{2.8}$$

$$|\partial \mathscr{W}'/\partial \boldsymbol{n}|^{-1} = \lambda^{\frac{1}{2}} |\partial \mathscr{W}/\partial \boldsymbol{n}|^{-1}, \tag{2.9}$$

and

$$\mathrm{d}\boldsymbol{s}' = \lambda\, \mathrm{d}\boldsymbol{s}. \tag{2.10}$$

Therefore, on the geometrically progressive polar grid of figure 1, where m_i is radial index and n_i is the angular index for the ith wavenumber, $\mathrm{d}\boldsymbol{s}$, $|\partial \mathscr{W}/\partial \boldsymbol{n}|^{-1}$ and $\mathscr{C}^2$ need only be calculated once for each different m_3-m_1 and $|n_3-n_1|$. Letting $\boldsymbol{k}_1 = (k_0, 0)$ and $\boldsymbol{k}_3$ vary over the entire grid, we initially construct a table of all possible values for $\mathrm{d}\boldsymbol{s}|\partial \mathscr{W}/\partial \boldsymbol{n}|^{-1}\mathscr{C}^2$. All other locus solutions, coupling coefficients, Jacobian terms, and phase space volumes can be obtained by appropriate rotation and multiplication of these results. For example if $|\boldsymbol{k}_1'-\boldsymbol{k}_3'| = \lambda^j|\boldsymbol{k}_1-\boldsymbol{k}_3|$, then

$$\mathrm{d}\boldsymbol{s}' \left|\frac{\partial \mathscr{W}'}{\partial \boldsymbol{n}}\right|^{-1} \mathscr{C}^2(\boldsymbol{k}_1', \boldsymbol{k}_2', \boldsymbol{k}_3', \boldsymbol{k}_4') = (\lambda)^{\frac{15}{2}j}\, \mathrm{d}\boldsymbol{s} \left|\frac{\partial \mathscr{W}}{\partial \boldsymbol{n}}\right|^{-1} \mathscr{C}^2(\boldsymbol{k}_1, \boldsymbol{k}_2, \boldsymbol{k}_3, \boldsymbol{k}_4). \tag{2.11}$$

These are exact scaling relationships inherent in the collision integral.

With the computation of $\mathscr{D}$ and integration around the locus $\boldsymbol{s}$, evaluation of the nonlinear transfer contour integral $\oint \mathscr{C}^2 \mathscr{D}\, |\partial \mathscr{W}/\partial \boldsymbol{n}|\, \mathrm{d}\boldsymbol{s}$ is then complete. Integration over all $\boldsymbol{k}_3$ values gives the nonlinear transfer source function $\partial n(\boldsymbol{k}_1)/\partial t$, as indicated in (2.3). This is also usually denoted $\mathscr{S}_{\mathrm{nl}}$. The scaling geometry of figure 1 allowed Tracy & Resio (1982) to obtain integration times that were typically over an order of magnitude less than integration times on regularly spaced grids. Using additional

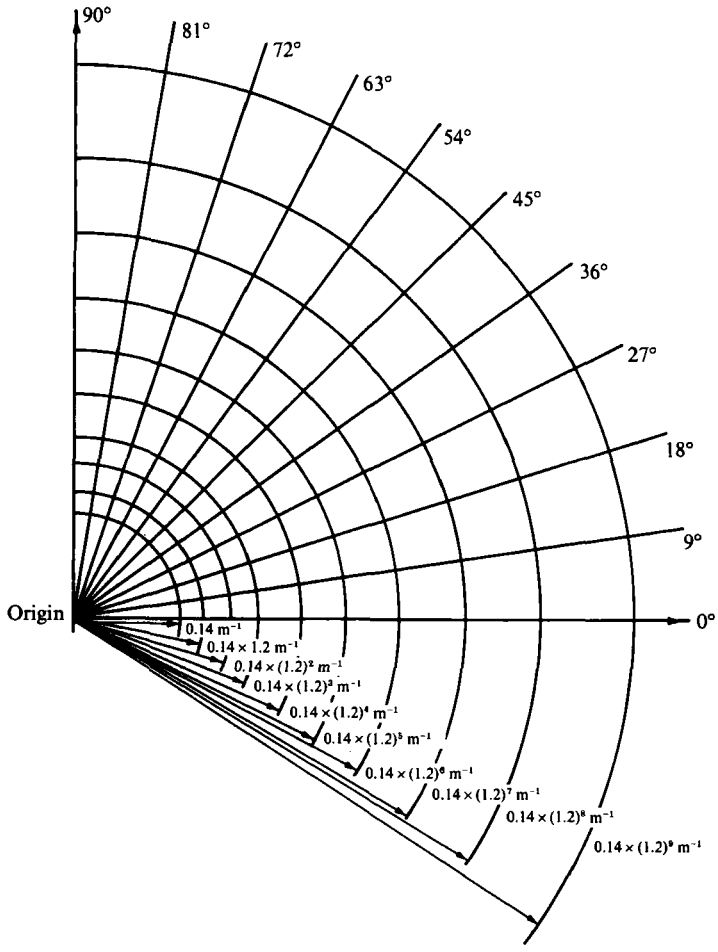

FIGURE 1. Polar grid in wavenumber space with radial intersection points spaced in the geometric progression $\boldsymbol{k}_{m+1} = \lambda \boldsymbol{k}_m$. This example uses $\boldsymbol{k}_0 = 0.14\ \mathrm{ms}^{-1}$ and $\lambda = 1.2$.

symmetries, such as permutations in $\boldsymbol{k}_1$ and $\boldsymbol{k}_3$, detailed evaluations of the collision integral for the entire spectrum can be performed in 20 min run times on an IBM-PC with an accelerator board, on grid resolutions comparable to Hasselmann & Hasselmann (1981).

In the work of Kitaigorodskii (1983), Resio (1987) and Toba *et al.* (1988), it appeared informative to examine fluxes of action (or energy) past a specific frequency ω_A in addition to looking at a source function for the entire spectrum. The integral for these fluxes from high to low frequencies may be written as

$$\Gamma(\omega_A) = \iiint \mathscr{C}^2 \mathscr{D} \left| \frac{\partial \mathscr{W}}{\partial \boldsymbol{n}} \right|^{-1} \mathrm{d}s\, H(|\boldsymbol{k}_3| - \boldsymbol{k}(\omega_A))\, H(\boldsymbol{k}(\omega_A) - |\boldsymbol{k}_1|)\, \mathrm{d}\boldsymbol{k}_3\, \mathrm{d}\boldsymbol{k}_1, \qquad (2.12)$$

where $H(x)$ is the Heaviside function, defined as

$$H(x) = \begin{cases} 1 & \text{for} \quad x \geqslant 0 \\ 0 & \text{for} \quad x < 0 \end{cases} \qquad (2.13)$$

and $k(\omega)$ is the wavenumber given by $k = \omega^2/g$. The corresponding nonlinear source function $\mathscr{S}_{\rm nl}$ can be obtained from a calculation of flux divergence whereas it is not possible to estimate the fluxes from the nonlinear source function. Flux estimates also provide a direct means of estimating all action transfers from one region of the spectrum to another. Consequently, they are useful in partitioning the percentage of action (or energy) that moves in various directions within the spectrum. The fact that we can compute positive fluxes from low to high frequencies as well as negative fluxes from high to low frequencies is very helpful in this regard.

3. Comparison of integration results to previous estimates

Most published results for the nonlinear wave–wave transfer have been restricted to spectra representable by the JONSWAP parameterization,

$$E(f) = \frac{\alpha g^2 f^{-5}}{(2\pi)^4} \exp\left(-1.25\frac{f}{f_{\rm p}}\right)\gamma^{\Xi}, \tag{3.1}$$

where

$$\Xi = \exp -\frac{1}{2}\left(\frac{f-f_{\rm p}}{\sigma f_{\rm p}}\right)^2. \tag{3.2}$$

These are typically converted to directional spectra by using the normalized $\cos^{2n}\theta$ form for angular spreading,

$$E_2(f,\theta) = E(f)\,\Lambda(n)\cos^{2n}\theta \tag{3.3}$$

where the normalization coefficient $\Lambda(n)$, satisfies

$$\int_{-\frac{1}{2}\pi}^{\frac{1}{2}\pi} \Lambda(n)\cos^{2n}\theta\,\mathrm{d}\theta = 1. \tag{3.4}$$

Figures 2(*a*)–2(*d*) compare the nonlinear transfer due to wave–wave interactions obtained from our integration method with results of Hasselmann & Hasselmann (1981). Parameters for all comparative spectra described by (3.1)–(3.4) are given in Table 1. The integration resolution in our computation was selected to be comparable to Hasselmann & Hasselmann (1981) in the spectral peak region. Consequently, any apparent differences in jaggedness in figures 2(*a*)–2(*d*) cannot be attributed to differences in grid resolution in this region of the spectrum.

Since we have not made any simplifying assumptions, our integration accuracy is limited only by the resolution of the integration grid. In figure 3 we compute the nonlinear transfer for the Pierson–Moskowitz spectrum considered in figure 2(*c*) using integration grids (i, j, k), where i is the number of wavenumber bins, $2j$ is the number of angular bins from $-120°$ to $+120°$ (unless otherwise specified) and k is the number of points on the locus specified in (2.5). Comparing integration grids (115, 60, 70), (78, 30, 50), (48, 20, 30) and (29, 10, 10), we find that (48, 20, 30) and (78, 30, 50) give results that are very close to those of (115, 60, 70). Not shown is the integration with 115 wavenumber bins, 360 angular bins from $-180°$ to $180°$ (1° discretization) and 70 points on the locus, which is essentially the same as (115, 60, 70). The effect of lower resolution on our integration method is a slightly less precise representation of the nonlinear transfer. All results are smooth.

The action flux formulation (2.12) implies that the rate of change of energy due to

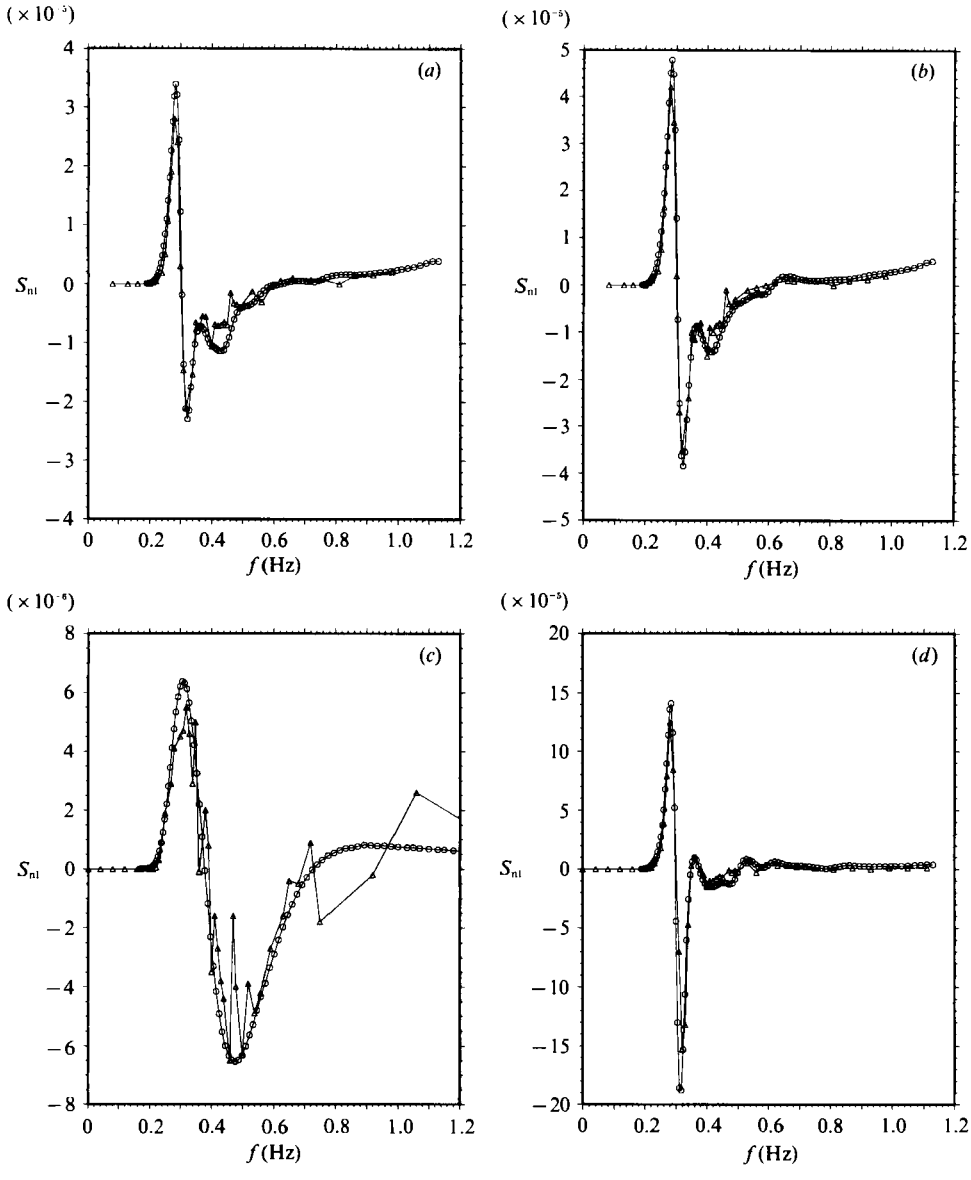

FIGURE 2. (*a*) Nonlinear transfer due to wave–wave interactions obtained from the integration method of this paper: ○, compared to Hasselmann & Hasselmann (1981); △, for case 2 in the latter study with $\cos^2\theta$ angular spreading. (*b*) As in (*a*) for Hasselmann & Hasselmann (1981) case 3 with angular spreading $\cos^4\theta$. (*c*) As in (*a*) for Hasselmann & Hasselmann (1981) case 13 corresponding to Pierson–Moskowitz spectrum. (*d*) As in (*a*) for Hasselmann & Hasselmann (1981) case 15 with $\gamma = 7$.

nonlinear transfer $\mathscr{S}_{nl}(f)$ may be written as the one-dimensional divergence of energy flux,

$$\mathscr{S}_{nl}(f) = \frac{\partial[\Gamma_E^+(f) + \Gamma_E^-(f)]}{\partial f}, \tag{3.5}$$

where $\Gamma_E^+(f)$ is the energy flux past f from low to high frequencies, and $\Gamma_E^-(f)$ is the energy flux past f from high to low frequencies. Numerically, we may compare this

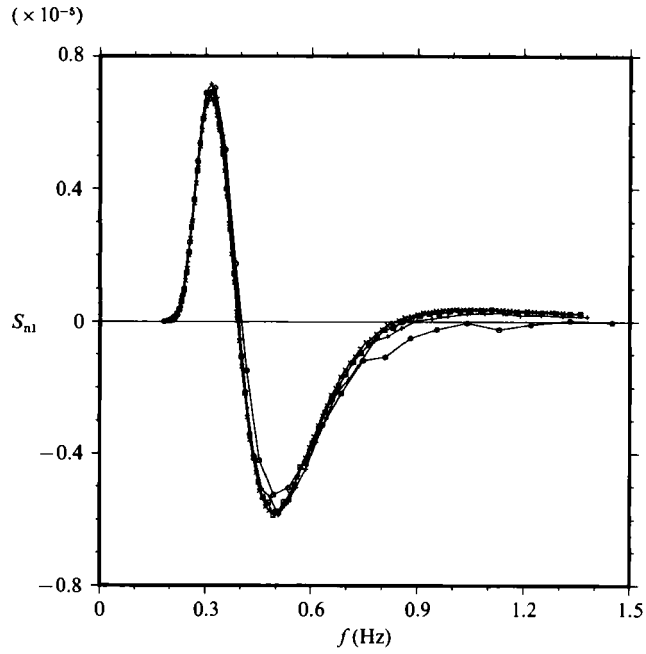

FIGURE 3. As in figure 2(*c*) for Pierson–Moskowitz spectrum, comparison the nonlinear transfer for integration grids (i, j, ℓ), using ×, (115, 60, 70); □, (78, 30, 50); +, (48, 20, 30); ○, (29, 10, 10), where i is the number of wavenumber bins, $2j$ is the number of angular bins from $-120°$ to $+120°$ and ℓ is the number of points on the locus.

Case†	Spreading function	Peakedness
2	$\frac{2}{\pi}\cos^2\theta$	3.3
3	$\frac{8}{3\pi}\cos^4\theta$	3.3
13	$\frac{2}{\pi}\cos^2\theta$	1.0
15	$\frac{2}{\pi}\cos^2\theta$	7.0

† From Hasselmann & Hasselmann (1981).

TABLE 1. Parameters for comparative spectra

flux divergence with the Boltzmann integral (2.3) for nonlinear transfer. Using the radial polar geometry of figure 1, we estimate the flux divergence centred between radial grid points where nonlinear transfer source term estimates are made,

$$\frac{\partial E(f)_{m+\frac{1}{2}}}{\partial t} = \frac{[\Gamma^+_{\rm E}(f)_m - \Gamma^+_{\rm E}(f)_{m+1}] + [\Gamma^-_{\rm E}(f)_{m+1} - \Gamma^-_{\rm E}(f)_m]}{f_{m+1} - f_m}. \tag{3.6}$$

Consequently, in regions of rapid nonlinear variations, the two calculations deviate

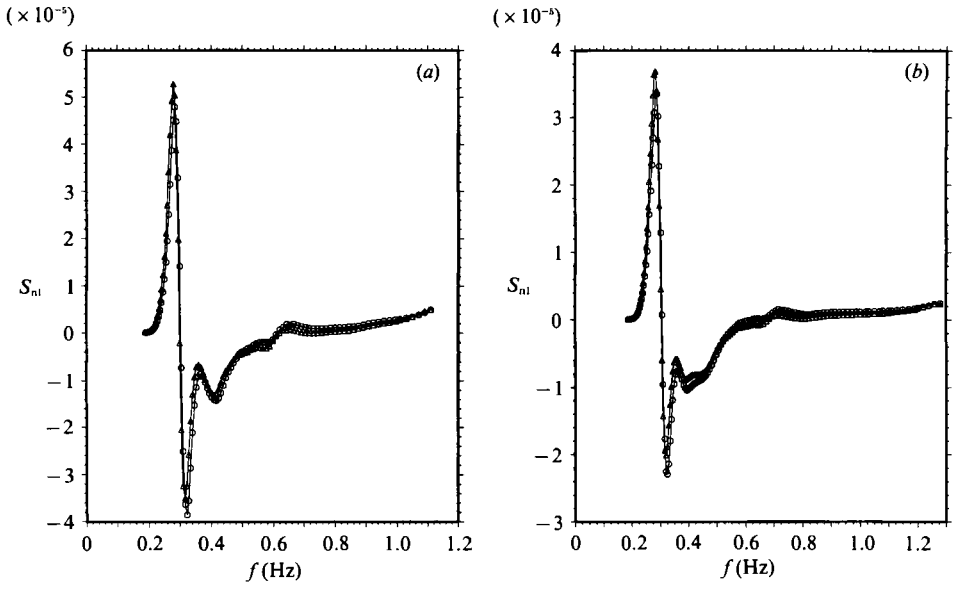

FIGURE 4. (*a*) A comparison between △, flux divergence, calculated by (3.5), and ○, the Boltzmann integral of (2.3), for Hasselmann & Hasselmann (1981) case 2. (*b*) As in (*a*) for Hasselmann & Hasselmann (1981) case 3.

slightly. As seen in figures 4(*a*) and 4(*b*), flux divergence estimates are a good approximation to estimates obtained directly from the Boltzmann integral. This confirms that the integration method for energy fluxes is properly posed and that the numerical technique has adequate detail.

Two-dimensional computations of $\partial n(\boldsymbol{k})/\partial t$, comparable with Webb (1978), are shown in figure 5. Two-dimensional energy fluxes through the wave spectrum can also be computed at each grid point and may be represented in terms of a flux density. For example, the action flux density into an element of phase space centred on $\boldsymbol{k}_1$ is

$$\Gamma_a(\boldsymbol{k}_1) = \int T(\boldsymbol{k}_1, \boldsymbol{k}_3)\, \hat{k}_{31}\, \mathrm{d}\boldsymbol{k}_3, \tag{3.7}$$

expressed in terms of a unit vector $\hat{\boldsymbol{k}}_{31}$ in the direction $\boldsymbol{k}_1 - \boldsymbol{k}_3$ and the transfer integral $T(\boldsymbol{k}_1, \boldsymbol{k}_3)$ defined in (2.4). The action flux in the positive x-direction into an element of phase space $\mathrm{d}\boldsymbol{k}_1$ centred on $\boldsymbol{k}_1$ is therefore

$$\Gamma_x^+(\boldsymbol{k}_1) = \mathrm{d}\boldsymbol{k}_1 \int T(\boldsymbol{k}_1, \boldsymbol{k}_3) \cos\theta_{31}\, \mathrm{d}\boldsymbol{k}_3, \tag{3.8}$$

and so forth for other components. Only contributions to the integral are allowed for which $T(\boldsymbol{k}_1, \boldsymbol{k}_3)\cos\theta_{31}$ is positive, where $\theta_{13} = \arctan[(k_{x_1} - k_{x_3})/(k_{y_1} - k_{y_3})]$. The usual Green's relation relates flux divergence to the energy change due to nonlinear wave–wave transfer. We plot the action flux density vectors in figure 6. These are for the high-frequency region of the spectrum considered in figure 2(*a*) using a 'moderate' resolution grid (50, 31, 46): 50 frequency bins, 4° discretization within the angular domain (−120°, +120°) and 46 points on the locus-resonance condition (2.5). It is evident that there is little nonlinear transfer outside the angular domain (−120°, +120°) and no flux across the x-axis.

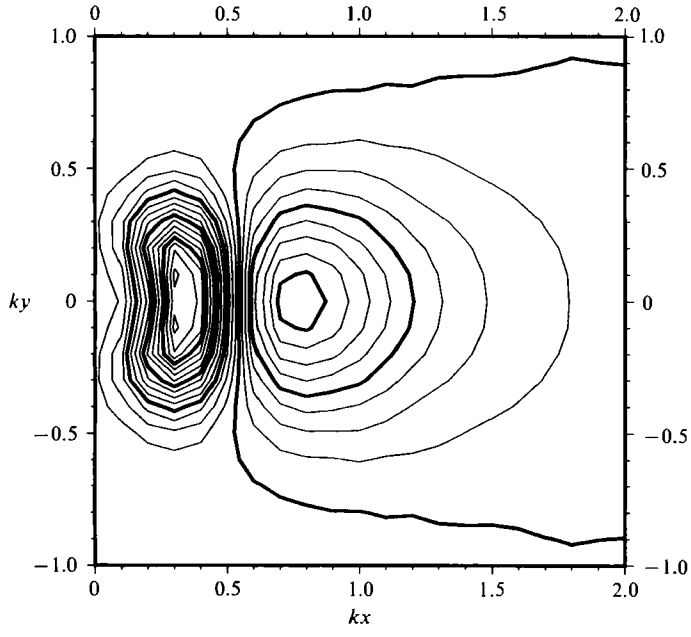

FIGURE 5. Two-dimensional nonlinear transfer $\partial n(\boldsymbol{k})/\partial t$ as a function of wavenumber, as in Webb (1978).

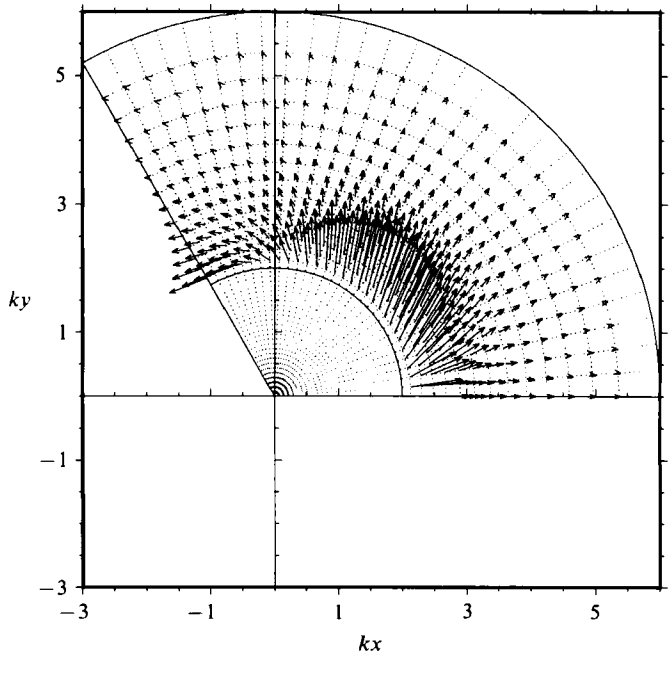

FIGURE 6. The two-dimensional nonlinear energy fluxes through the spectrum in the high-frequency region of the spectrum in figure 2(*a*). The magnification factor is 1.4×10^7.

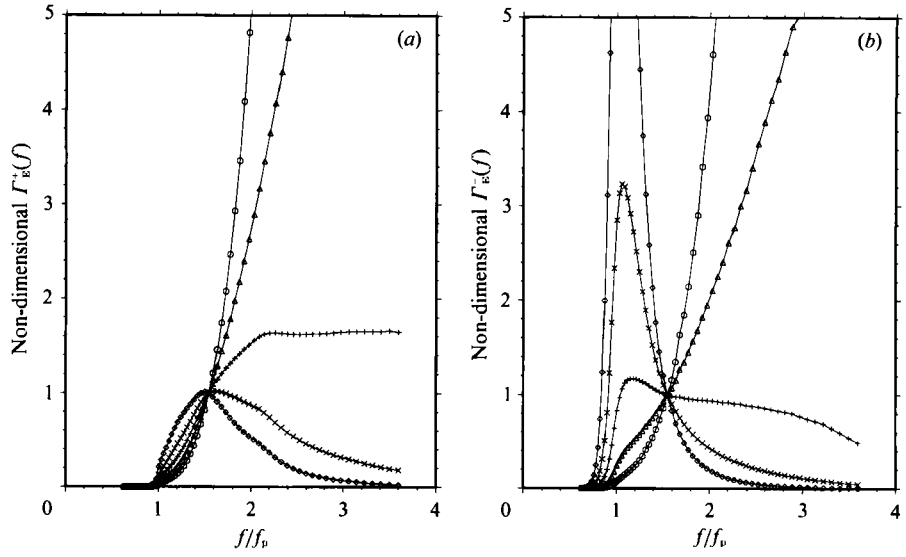

FIGURE 7. (*a*) Variations of energy flux to high frequencies Γ_E^+ with different equilibrium range power laws normalized by the value each has at $1.6f_p$: ○, for f^{-2}, △, for f^{-3}; +, for f^{-4}; ×, for f^{-5}; ◇, for f^{-6}. Other parameters are $f_p = 0.3$, $\gamma = 1.214$, $\alpha_4 u = 0.01$, $\sigma_a = 0.07$, $\sigma_b = 0.09$ and directional spreading is $\cos^2\theta$. (*b*) Variations of energy flux to low frequencies Γ_E^- as a function of equilibrium range power law as in (*a*).

4. Basic scaling behaviour of nonlinear fluxes

4.1. *Flux dependence on power laws in the equilibrium range*

To examine the energy flux behaviour for different equilibrium range power laws, we consider simple specta of the form

$$E(f,\theta) = \Lambda\alpha_4 u g f^{-m}\psi\left(\frac{f}{f_p}\right)\cos^2\theta, \tag{4.1}$$

where m is a positive integer, $\alpha_4 u$ is a dimensional constant with units of length/time, Λ is a directional normalization constant satisfying

$$\int_{-\frac{1}{2}\pi}^{\frac{1}{2}\pi} \Lambda\cos^2\theta\,\mathrm{d}\theta = 1 \tag{4.2}$$

and ψ is a non-dimensional shape function specified by the usual JONSWAP-type parameters (3.1)–(3.4), and prescribed in subsequent sections. Experimental evidence suggests that the equilibrium range exists in a subrange of the spectrum from approximately $1.6f_p$ to $2.6f_p$. To accentuate the divergence aspects of energy fluxes, we normalize all fluxes for a given power law by its value at the low-frequency limit of the equilibrium range (i.e. at about $1.6\,f_p$). Figures 7(*a*) and 7(*b*) show the behaviour of these normalized fluxes to high frequencies $\Gamma_E^+(k)$ and low frequencies $\Gamma_E^-(k)$ for various power laws. Unless otherwise specified, parameters are $f_p = 0.3$, $\gamma = 1.214$, $\alpha_4 u = 0.01$, $\sigma_a = 0.07$, $\sigma_b = 0.09$ and directional spreading is $\cos^2\theta$ in this and subsequent sections. For a constant energy flux through the equilibrium range of the spectrum, the normalized fluxes should retain a value of approximately 1. However, as can be seen in figure 7, the fluxes are approximately constant only for an f^{-4} spectrum. Spectra with f^{-2} and f^{-3} equilibrium ranges have fluxes which

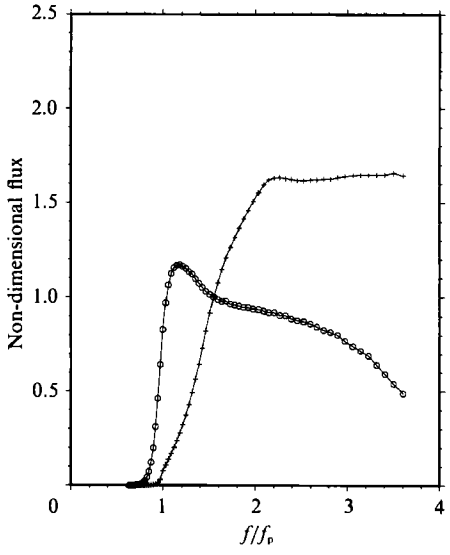

FIGURE 8. Variations of energy flux to high frequencies Γ_E^+, and to low frequencies Γ_E^-, as a function of different peak frequencies: 0.2, 0.3, 0.4 Hz.

increase with increasing frequency. Spectra with f^{-5} and f^{-6} equilibrium ranges have fluxes which decrease with increasing frequency.

The calculations shown here provide additional support for the existence of an f^{-4} equilibrium range in wave spectra. For the remainder of this study, we restrict ourselves to analyses of spectra with f^{-4} equilibrium ranges. The equation for this class of spectra is

$$E(f,\theta) = A\alpha_4 u g f^{-4} \psi\left(\frac{f}{f_p}\right)\cos^2\theta. \tag{4.3}$$

As discussed in Resio & Perrie (1989), a judicious selection of parameters makes such a form equivalent to the JONSWAP spectral form.

4.2. *Flux dependence on variations in peak frequency*

To investigate the behaviour of energy fluxes through the equilibrium range as a function of peak frequency, we consider spectra of the form (4.3) with ψ given by

$$\psi\left(\frac{f}{f_p}\right) = \begin{cases} \left(\dfrac{f}{f_p}\right)^4 \exp\left(1-\left(\dfrac{f_p}{f}\right)^4\right) & \text{for } f \leqslant f_p, \\ 1 & \text{for } f \geqslant f_p. \end{cases} \tag{4.4}$$

Integrations for peak frequencies f_p of 0.2, 0.3 and 0.4 show that energy fluxes are identical when plotted as a function of f/f_p. Figure 8, which appears to contain only two curves, actually contains plots for the fluxes to both high and low frequencies through all three spectra.

This may seem surprising at first, since Hasselmann *et al.* (1973) established that nonlinear transfer due to wave–wave interactions is dependent on f_p. However, the frequency axis in figure 8 is scaled by f_p. The nonlinear transfer source function for these spectra has the form

$$\mathcal{S}_{nl} \sim f_p^{-1}, \tag{4.5}$$

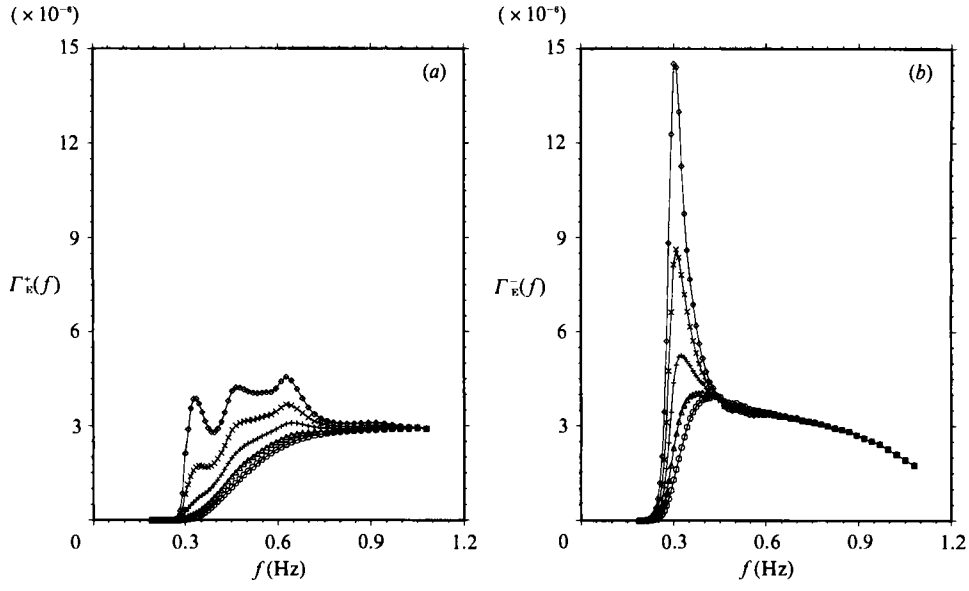

FIGURE 9. (*a*) Variations of energy flux to high frequencies Γ_E^+ with peakedness: ○, for $\gamma = 0.65$; △, for $\gamma = 1.0$; +, for $\gamma = 1.55$; ×, for $\gamma = 2.30$; ◇, for $\gamma = 3.25$. (*b*) Variations of energy flux to low frequencies Γ_E^- with peakedness as in (*a*).

whereas for an f^{-5} spectrum

$$\mathscr{S}_{nl} \sim f_p^{-4}. \tag{4.6}$$

4.3. *The influence of the spectral peak on fluxes*

In this section we consider the influence of the sharp energy cutoff below the spectral peak as well as the manner in which variations in spectral peakedness affect energy fluxes through the spectrum. Our spectra are of the form (4.2), with ψ given by

$$\psi\left(\frac{f}{f_p}\right) = \begin{cases} \left(\frac{f}{f_p}\right)^4 \exp\left(1-\left(\frac{f_p}{f}\right)^4\right)\gamma^{\Xi} & \text{for } f \leqslant f_p, \\ \gamma^{\Xi} & \text{for } f > f_p, \end{cases} \tag{4.7}$$

where

$$\Xi = \exp -\frac{1}{2}\left(\frac{f-f_p}{\sigma f_p}\right)^2, \tag{4.8}$$

and γ is a non-dimensional peakedness parameter.

The variation in energy fluxes for $\gamma = 0.65$, 1.0, 1.55, 2.30 and 3.25 is shown in figure 9. This range of γ corresponds to the measurements of Donelan, Hamilton & Hui (1985). Figure 10 show the corresponding nonlinear energy transfer for these spectra. A notable feature is the shift of the positive lobe toward higher frequencies as γ decreases, particularly when γ becomes less than 1. The associated transfers of action and momentum to the forward face also vary markedly as a function of γ. This is an important mechanism in controlling wave growth and possibly the evolution into a fully-developed spectral form.

Approximations by Kitaigorodskii (1983) and Resio (1987) concerning equilibrium range fluxes neglected consideration of the extent to which energy transfers are influenced by the spectral peak and the associated cutoff energy on the forward face

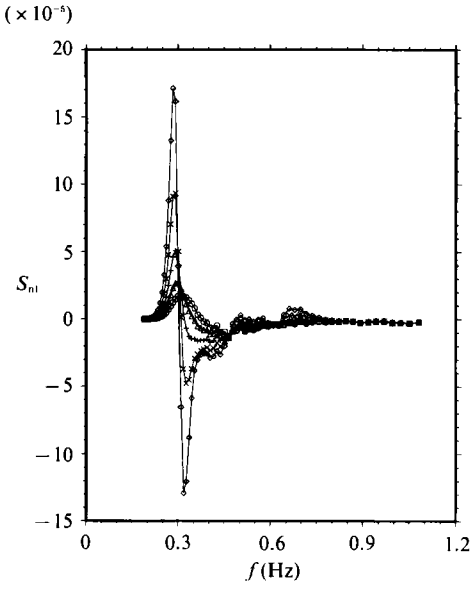

FIGURE 10. As in figure 9 for corresponding nonlinear transfer.

of the spectrum. Experimental results suggest large departures from equilibrium range for frequencies less than $1.6f_p$ (figure 15 in Donelan *et al.* 1985). To examine the influence of the spectral peak, we consider normalized energy fluxes through the spectrum as a function of non-dimensional frequency f/f_p. The normalization is that proposed for equilibrium range fluxes by Resio (1987) where it was shown that energy fluxes in the equilibrium range should vary as

$$\Gamma_E(k) \approx \epsilon \frac{g^2 F^3(k)\, k^9}{\omega^3} \tag{4.9}$$

letting $F(k)$ be the one-dimensional energy density in wavenumber space and ϵ, a non-dimensional constant. We therefore define normalized energy fluxes to be

$$\hat{\Gamma}_E(k) = \frac{\Gamma_E(k)\,\omega}{g^2 F^3(k)\, k^9} \tag{4.10}$$

Figure 11 shows the behaviour of $\hat{\Gamma}^{\pm}_E(k)$ as a function of f/f_p for different values of γ. From figure 11(*a*), the normalized flux to high frequencies $\hat{\Gamma}^{+}_E(k)$ attains equilibrium range values that are essentially independent of γ by $f/f_p \approx 2.3$. Figure 11(*b*) implies that the normalized flux to low frequencies $\hat{\Gamma}^{-}_E(k)$ attains equilibrium range values that are essentially γ independent by $f/f_p \approx 1.5$.

Finally, we consider the magnitude of nonlinear energy fluxes and their associated source terms as a function of spectral peakedness. Hasselmann *et al.* (1973) suggest that as the peakedness of the spectrum increases, the source functions become larger. While this may be true, the mechanism behind it may not be the 'sharpness' of the spectrum. It may be due to the fact that, in the spectral parameterization used in this study and by Hasselmann *et al.* (1973), the absolute magnitude of the energy densities in the region of the peak increases with increasing γ. As these energy densities increase, their contributions to the nonlinear fluxes increase by $F^3(k)$ and the divergences of the fluxes also increase.

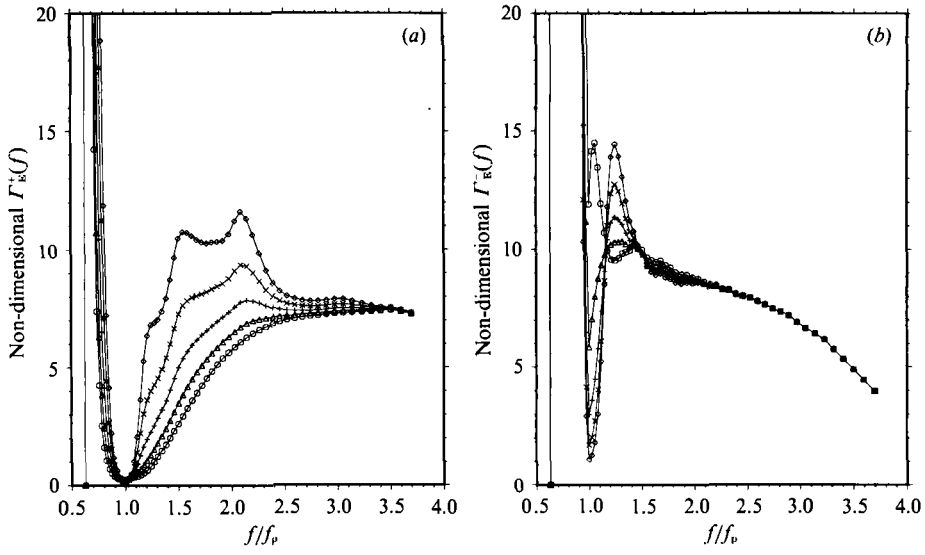

FIGURE 11. (*a*) Variations in non-dimensional flux to high frequencies $\hat{\Gamma}_E^+(k)$ with respect to peakedness as in figure 9, plotted against f/f_p. $\hat{\Gamma}_E^+(k)$ is non-dimensionalized according to (4.10). (*b*) Variations in non-dimensional flux to low frequencies $\hat{\Gamma}_E^-(k)$ with respect to peakedness as in (*a*).

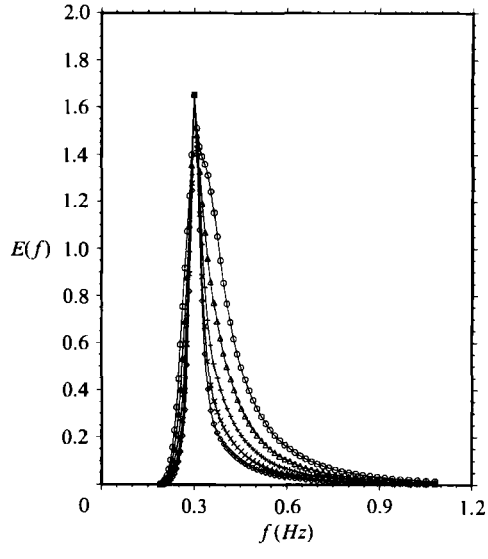

FIGURE 12. Variation of spectra with respect to peakedness as in figure 9. All spectra are normalized to have the same maximum.

A related concern is therefore whether or not source terms and fluxes become larger for different peakedness values, given the same energy density at the spectral peak. To answer this, we performed integrations for spectra defined by (4.3), (4.7)–(4.8) and normalized to have the same spectral energy at the peak. Figure 12 shows the spectral shapes for various γ generated in this manner. The fluxes and associated nonlinear energy transfer terms are shown in figures 13 and 14

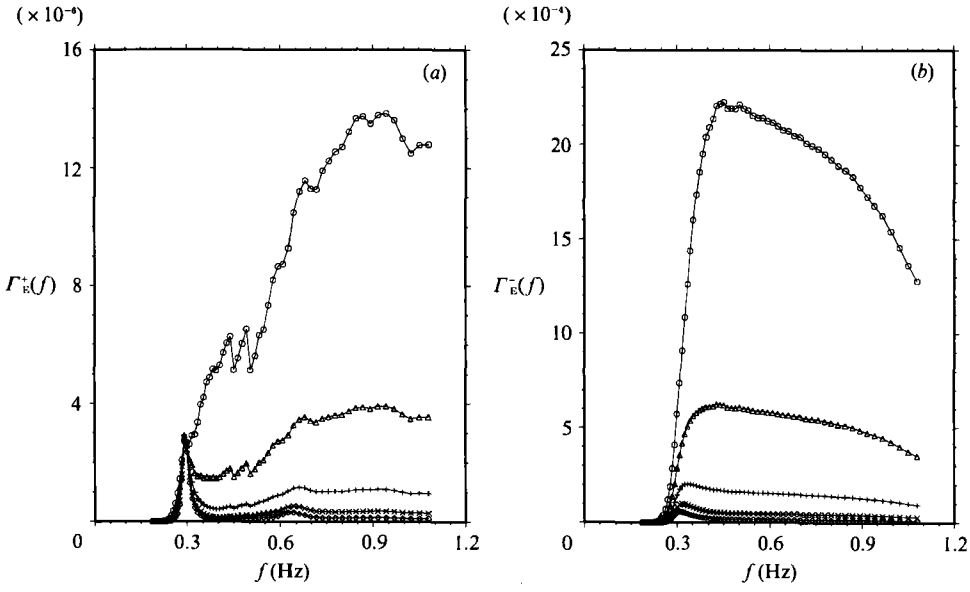

FIGURE 13. (*a*) Energy fluxes to high frequencies $\Gamma_E^+(k)$ corresponding to spectra of figure 12 as a function of peakedness as in figure 9. (*b*) Energy fluxes to low frequencies $\Gamma_E^-(k)$ as a function of peakedness as in (*a*).

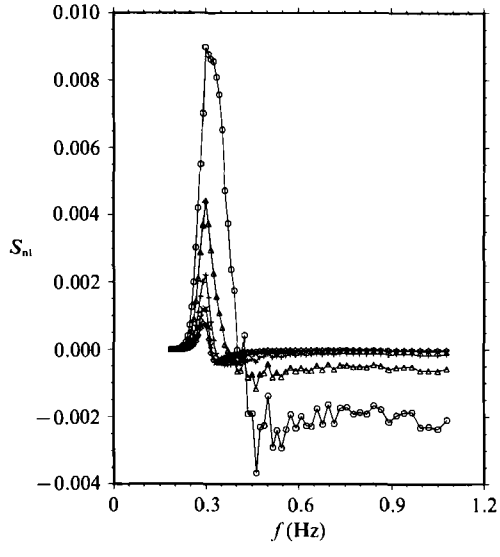

FIGURE 14. Nonlinear transfer corresponding to the spectra of figure 12.

respectively. It is evident that, with the same energy density at the spectral peak, the magnitude of both the fluxes and the source terms are larger for broader spectra than they are for more sharply peaked spectra.

4.4. *Effects of angular distribution of energy on energy fluxes*

The parameterization of spectral peakedness presented above gives an indication of the manner in which the gradient of energy density as a function of frequency f, can affect energy fluxes through a spectrum. For a given frequency, the gradient of energy density with angle θ can also affect energy fluxes through a spectrum. Thus

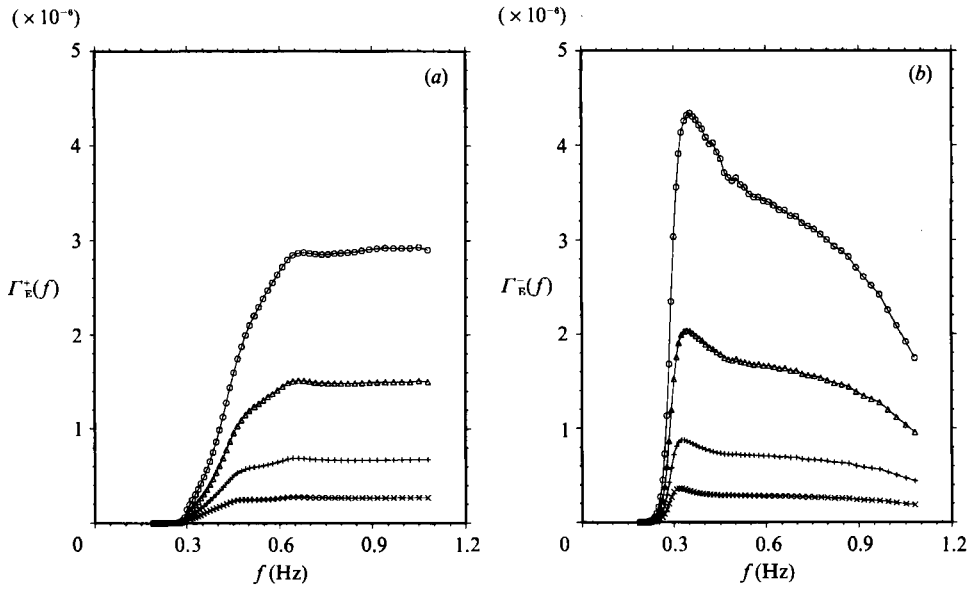

FIGURE 15. (*a*) Energy fluxes to high frequencies $\Gamma_E^+(k)$ as a function of angular spreading $\cos^{2n}\theta$: ×, for $n = 1$; +, for $n = 2$; △, for $n = 4$; ○, for $n = 8$. (*b*) Energy fluxes to low frequencies $\Gamma_E^-(k)$ as a function of angular spreading as in (*a*).

far, we have only considered spectra with a $\cos^2\theta$ angular distribution. Although it may be instructive to analyse spectra with f- and θ-dependent spreading functions as presented by Mitsuyasu *et al.* (1975), Hasselmann, Dunkel & Ewing (1980) and Donelan *et al.* (1985), for simplicity we examine only spreading functions which are independent of f.

Using the spectrum (4.3) and (4.7)–(5.8) with $\alpha_4 u = 0.01$, $f_p = 0.3$, $\gamma = 1.214$, $\sigma_a = 0.07$ and $\sigma_b = 0.09$, integrations were made with normalized $\cos^{2n}\theta$ spreading functions, letting n equal 1, 2, 4 and 8. As shown in figure 15, energy fluxes are dependent on the angular spreading function and increase as n increases. The dependency is not as strong as in the case of spectral peakedness although the range of variation was taken to cover the range that could be expected to occur in nature. The equilibrium range first occurs at $f/f_p \approx 2.0$ for the flux to high frequencies $\Gamma_E^+(k)$ and somewhat earlier at $f/f_p \approx 1.5$ for the flux to low frequencies $\Gamma_E^-(k)$.

4.5. *Variations in nonlinear fluxes due to the equilibrium range coefficient*

It is apparent from the algebraic structure of the density function $\mathscr{D}$ as shown in (2.2), that any multiplicative factor introduced into a spectral density manifests itself as the cube of that factor in $\mathscr{D}$. As this is used later, we numerically demonstrate this. Figure 16 shows the calculated energy fluxes for a reference f^{-4} spectrum with parameter $\alpha_4 u = 0.01$, $f_p = 0.3$, $\gamma = 1.21$, $\sigma_a = 0.07$ and $\sigma_b = 0.09$. Energy fluxes are also presented for spectra with identical parameters except that $\alpha_4 u = 0.03$. Dividing the fluxes of the second computation by 27 makes the two curves exactly the same.

4.6. *Numerical evaluation of the non-dimensional flux coefficients*

Figure 9 showed that the flux to high frequencies $\Gamma_E^+(k)$ attains equilibrium range values that are independent of peakedness γ by $f/f_p \approx 2.3$ and the flux to low frequencies $\Gamma_E^-(k)$ attains equilibrium range values that are γ independent by $f/f_p \approx$

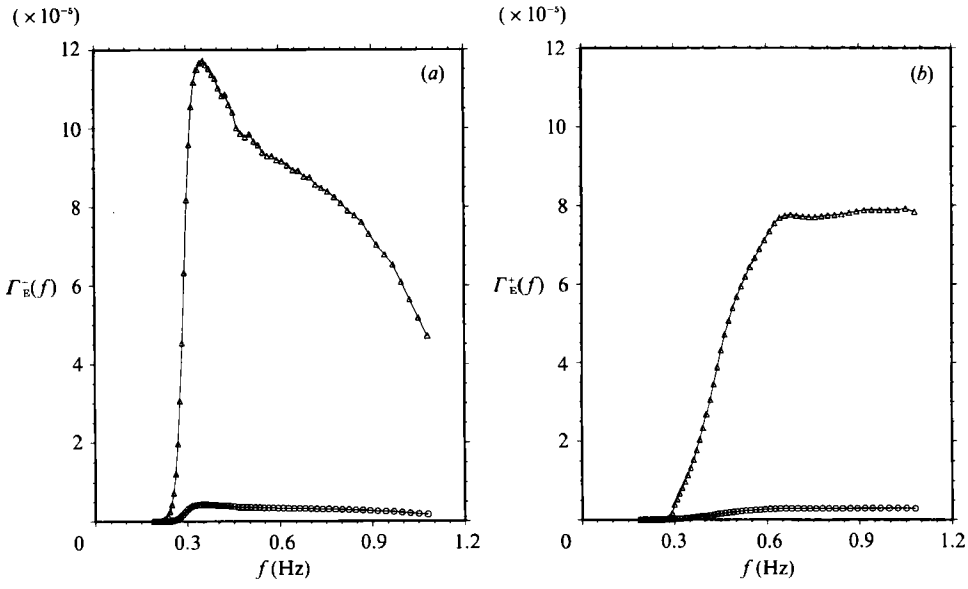

FIGURE 16. (*a*) Variation of energy fluxes to high frequencies $\Gamma_E^+(k)$ with $\alpha_4 u$: ○, for $\alpha_4 u = 0.01$; △, for $\alpha_4 u = 0.03$. The plots differ by a factor of 27. (*b*) Variation of energy fluxes to low frequencies $\Gamma_E^-(k)$ as a function of $\alpha_4 u$ as in (*a*).

1.5. Figure 8 shows that these fluxes are independent of the location of f_p. Therefore, for a given angular spreading function, whether or not frequency dependent, energy fluxes in these equilibrium ranges are only dependent on the equilibrium range coefficient. This supports the estimates for energy fluxes through the spectrum made by Kitaigorodskii (1983) and Resio (1987), based on arguments that the fluxes should approximately balance energy input by wind.

Energy flux estimates (4.9) expressed in terms of frequency, may be represented as

$$\Gamma_E^{\pm}(f) = \frac{\epsilon^{\pm}(2\pi)^9 f^{12} E^3(f)}{8g^4} \phi^{\pm}\left(\frac{f}{f_p}\right) \tag{4.11}$$

where ' + ' refers to fluxes from low to high frequencies, ' − ' refers to fluxes from high to low frequencies, $\phi^{\pm}$ is a non-dimensional shape function and $\epsilon^{\pm}$ is a non-dimensional constant. As $\phi^{\pm} = 1$ in the equilibrium range, $\epsilon^{\pm}$ has the same meaning as ϵ in (4.9).

Substituting the appropriate equilibrium form for $E(f)$ from (4.3) into (4.11) yields,

$$\Gamma_E^{\pm}(f) = \epsilon^{\pm} \frac{\alpha_4^3 u^3 (2\pi)^9 A^3}{8g} \tag{4.12}$$

which, as shown in figure 9, represent good approximations for all spectra of the form (4.3). Since $\alpha_4 u$ is a known quantity in our integrations, we can explicitly evaluate $\epsilon^{\pm}$. We find

$$\epsilon^{\pm} \approx 60 \tag{4.13}$$

making the evaluation at about the midpoint of the equilibrium range. This is consistent with the earlier estimates of Resio (1987).

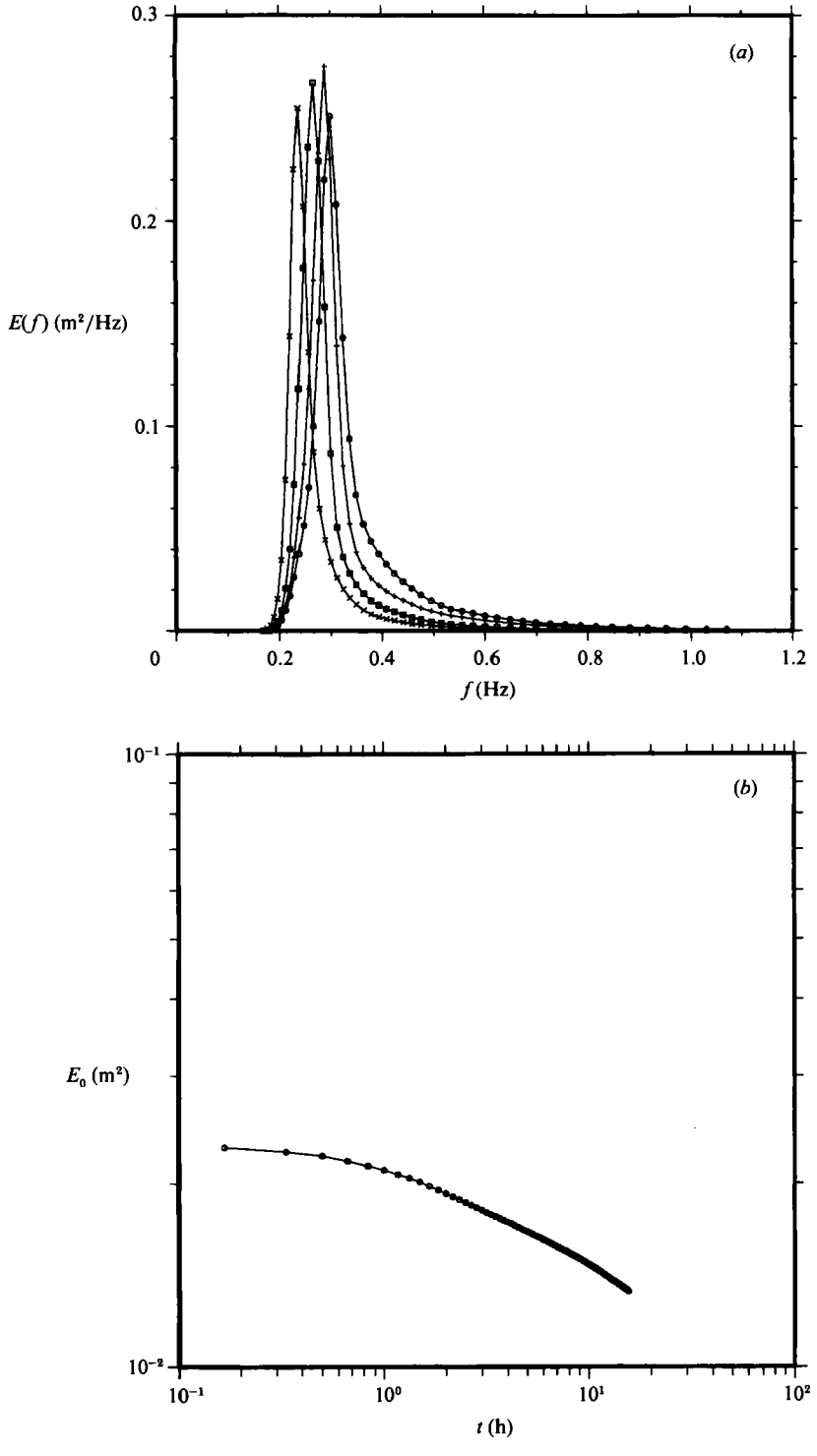

FIGURE 17. For caption see next page.

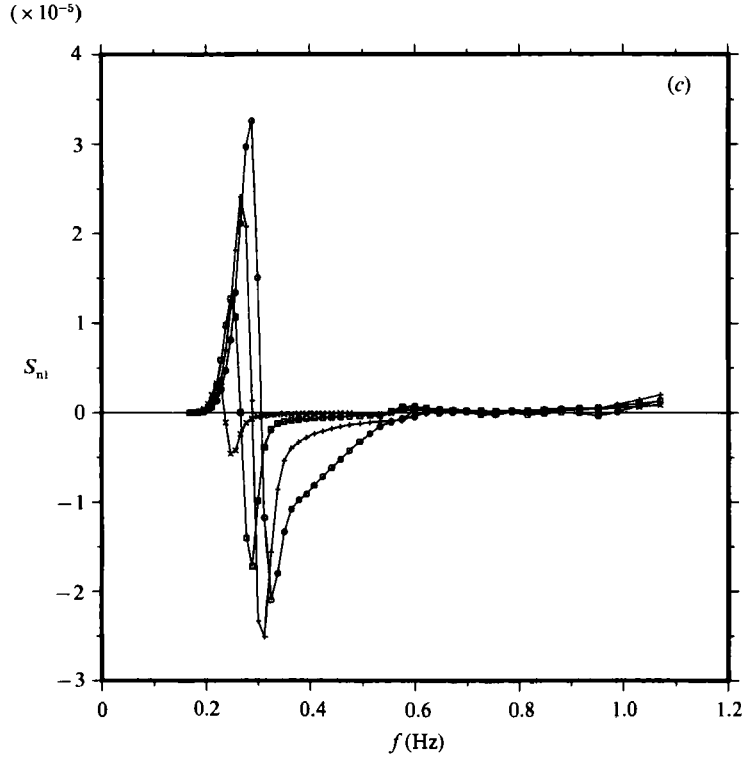

FIGURE 17. (*a*) The time evolution of one-dimensional energy $E(f)$ in the absence of $\mathscr{S}_{in}$ and $\mathscr{S}_{ds}$. The integration grid is (48, 20, 30) with 15 s timesteps. ○, 15 s; +, 1 h; □, 3 h; ×, 11 h. (*b*) As in (*a*), the total energy E_0 variation with time. (*c*) As in (*a*), the variation of the nonlinear energy transfer $\mathscr{S}_{nl}$ with time.

5. Spectral evolution in time

5.1. *Evolution of energy and nonlinear transfer in time*

With respect to space and time, the spectral energy density $E(f,\theta)$ from (4.3) in deep water evolves as

$$\frac{\partial E}{\partial t}(f,\theta)+\boldsymbol{C}_g\cdot\nabla E(f,\theta)=\mathscr{S}_{in}+\mathscr{S}_{nl}+\mathscr{S}_{ds} \tag{5.1}$$

where $\mathscr{S}_{in}$ is the wind input spectral energy, $\mathscr{S}_{nl}$ is the nonlinear transfer due to wave–wave interactions and $\mathscr{S}_{ds}$ is the wave breaking dissipation. We compute the time evolution of one-dimensional energy $E(f)$, total energy E_0 and nonlinear transfer $\mathscr{S}_{nl}$ in figures 17 (*a*), 17 (*b*) and 17 (*c*), in the absence of $\mathscr{S}_{in}$ and $\mathscr{S}_{ds}$. Our integration grid is (48, 20, 30), with 30 s timesteps and an initial spectrum as shown in figure 17 (*a*). We model the spectrum above $2f_p$ with an f^{-4} tail to reduce computer requirements.

The time progression of the spectrum is presented in figure 17 (*a*). Influenced only by wave–wave interactions, the spectrum initially steepens and the peak migrates to lower frequencies. However, because the integration grid extends over only a finite range on the frequency axis, total energy slowly decreases as energy is fluxed to the high-frequency boundary of the grid and is lost to the next timestep of the integration. Thus, the peak of the spectrum decreases with time after about an hour. The time evolution of total energy E_0 in figures 17 (*b*) is a further reflection of the loss

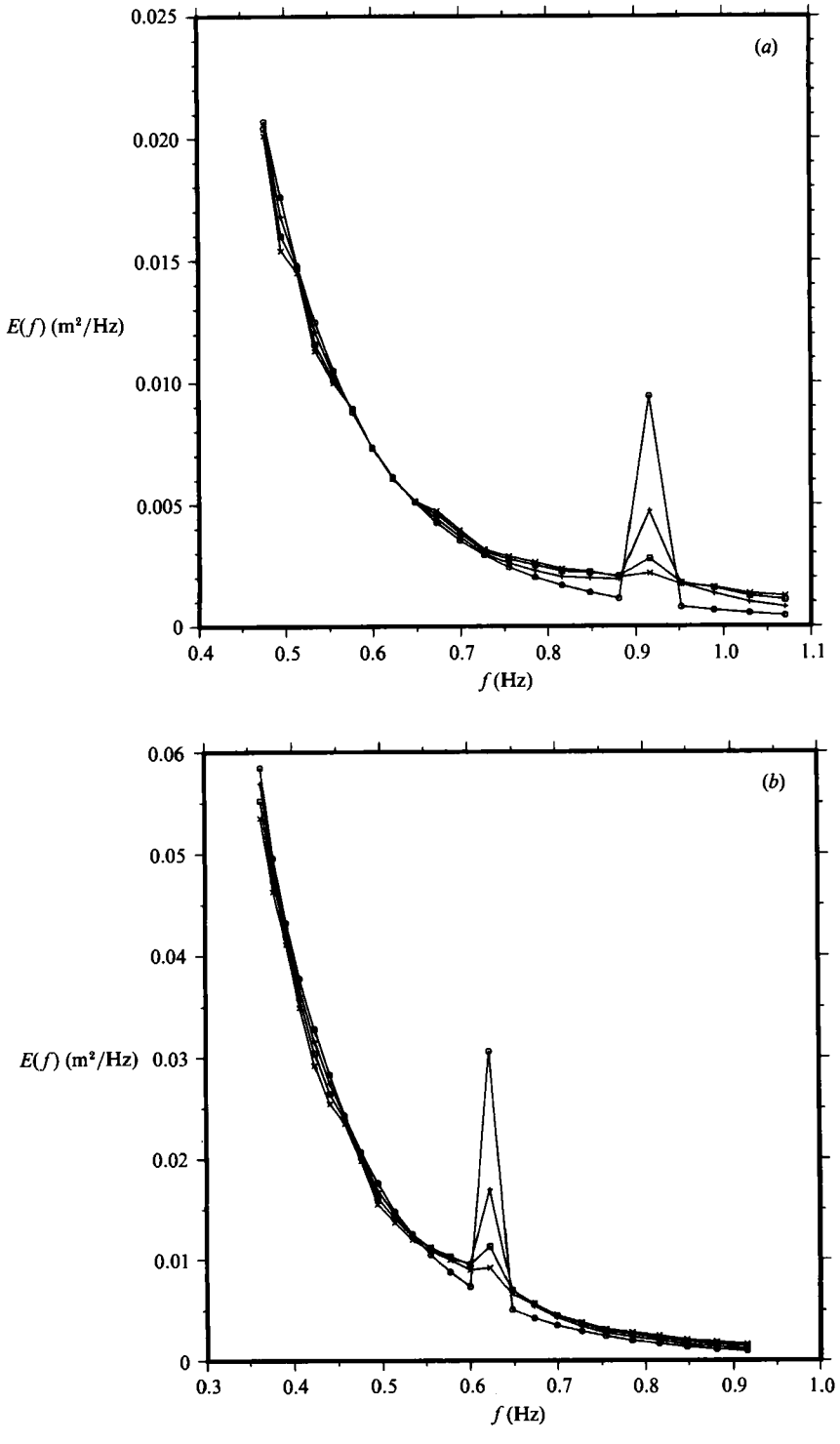

FIGURE 18. For caption see next page.

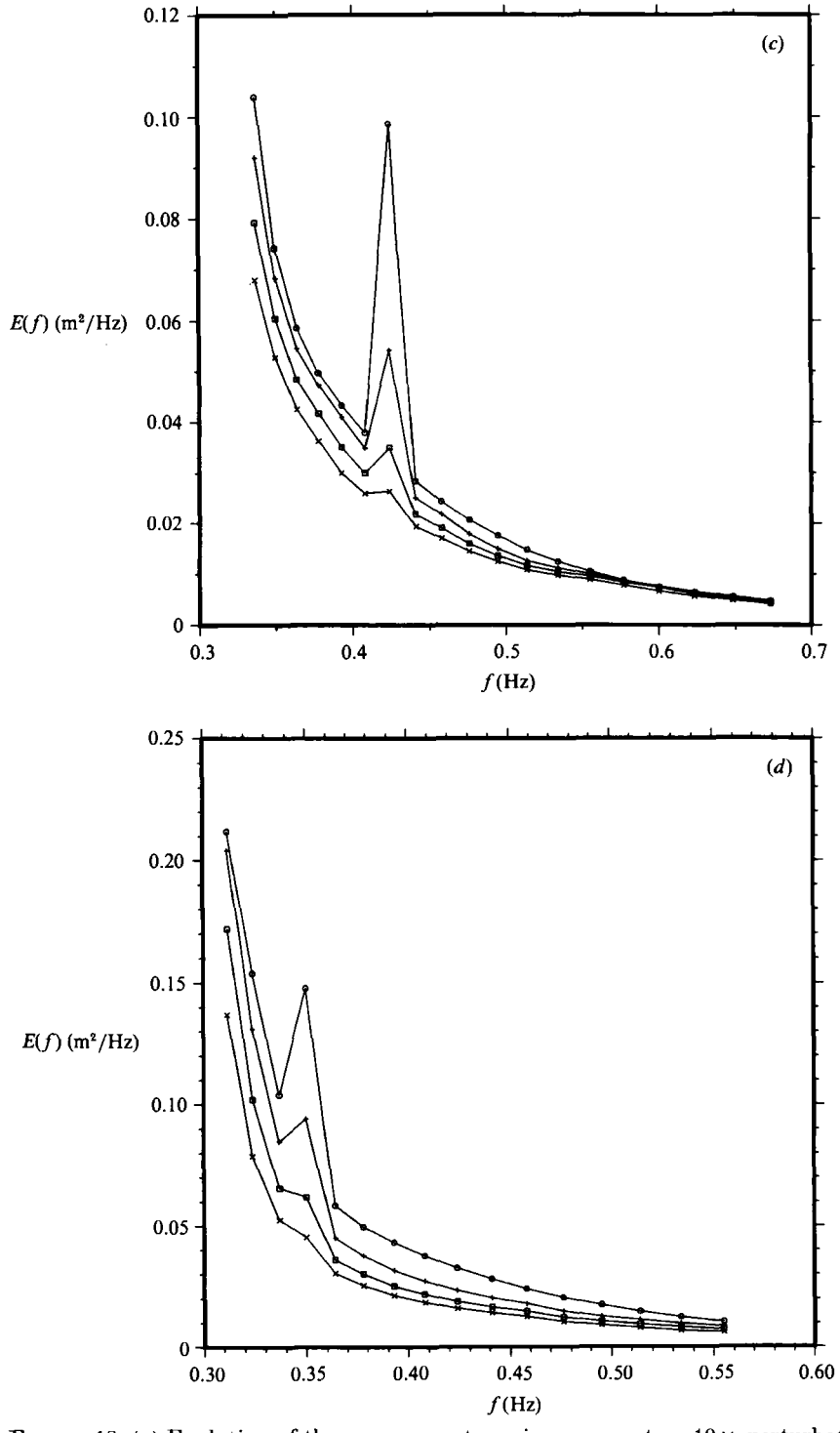

FIGURE 18. (*a*) Evolution of the energy spectrum in response to a 10× perturbation at $3f_p$ where the spectrum is denoted by: ○, initially; +, after 1 min; □, after 2 min; ×, after 3 min. (*b*) As in (*a*) in response to a 5× perturbation at $2f_p$ where the spectrum is denoted by: ○, initially; +, after 2 min; □, after 4 min; ×, after 6 min. (*c*) As in (*a*) in response to a 3× perturbation at $1.5f_p$ where the spectrum is denoted by: ○, initially; +, after 10 min; □, after 20 min; ×, after 30 min. (*d*) As in (*a*) in response to a 2× perturbation at $\frac{7}{8}f_p$ where the spectrum is denoted by: ○, initially; +, after 20 min; □, after 40 min; ×, after 60 min.

of energy due to finiteness of the grid. Finally, in figure 17(*c*) we see the evolution of the corresponding nonlinear transfer $\mathscr{S}_{\rm nl}$. Owing to a diminished spectrum, $\mathscr{S}_{\rm nl}$ decreases drastically as time increases and migrates to lower frequencies following the migration of the spectrum.

5.2. *Response to perturbations in the spectrum*

It is important to investigate the response of the nonlinear energy transfer to perturbations within the spectrum in order to assess the rate at which a spectrum relaxes toward a quasi-stationary state. We compute the time evolution of one-dimensional energy $E(f)$ using a (48, 20, 30) grid with initial spectral parameters as in §5.1. In figure 18(*a*), we introduce a 10 × perturbation at $3f_{\rm p}$. Using 15 s timesteps and integrating over the entire frequency domain (without using an f^{-4} tail as in §5.1), we see that within 3 min the nonlinear interactions have reduced the perturbation to less than 90% of its original magnitude and distributed the energy among neighbouring spectral energy bins. Figure 18(*b*) presents a 5 × perturbation at $2f_{\rm p}$. In this situation, the nonlinear interactions essentially remove the perturbation within 6 min. In figure 18(*c*) a 3 × perturbation at $1.5f_{\rm p}$ is removed in 30 min. Finally in figure 18(*d*) a 2 × perturbation at $\frac{1}{8}f_{\rm p}$ requires 1 h before nonlinear interactions have removed approximately 90% of it.

From figure 3, our investigations show that the nonlinear energy transfer should be smooth, even for very coarse integration grids. We have demonstrated that nonlinear wave–wave interactions work to smooth perturbations introduced into the spectrum as spikes. Clearly the time taken for the nonlinear interactions to respond to any perturbation depends strongly on where it occurs within the spectrum.

5.3. *Relaxation times within the equilibrium range*

An alternate view of the spectral response to perturbations within the equilibrium range may be presented in terms of relaxation times within the equilibrium range. In a manner typical of many others. Kitaigorodskii (1983) estimated relaxation times for wave–wave interactions in terms of energy density and rate of change of energy, at a given frequency

$$\mathscr{T} = \frac{E(f)}{\dfrac{\partial E(f)}{\partial t}}. \tag{5.2}$$

Unfortunately, the denominator of (5.2) becomes very small in the equilibrium range and the estimated relaxation time becomes arbitrarily large. Therefore we propose a different form based on energy fluxes

$$\mathscr{S} = \frac{\mathscr{E}}{\Gamma_{\rm E}^{+} + \Gamma_{\rm E}^{-}}, \tag{5.3}$$

where $\mathscr{E}$ is the total energy in the region of the spectrum being considered,

$$\mathscr{E} = \int_{f_1}^{f_2} E(f)\,{\rm d}f, \tag{5.4}$$

and f_1 and f_2 are the appropriate upper and lower frequency limits of the equilibrium range. This definition relates relaxation time to the time required for nonlinear energy fluxes to remove all the energy from a specific region of the spectrum. This is a physically consistent approach to estimating the relative strength of the

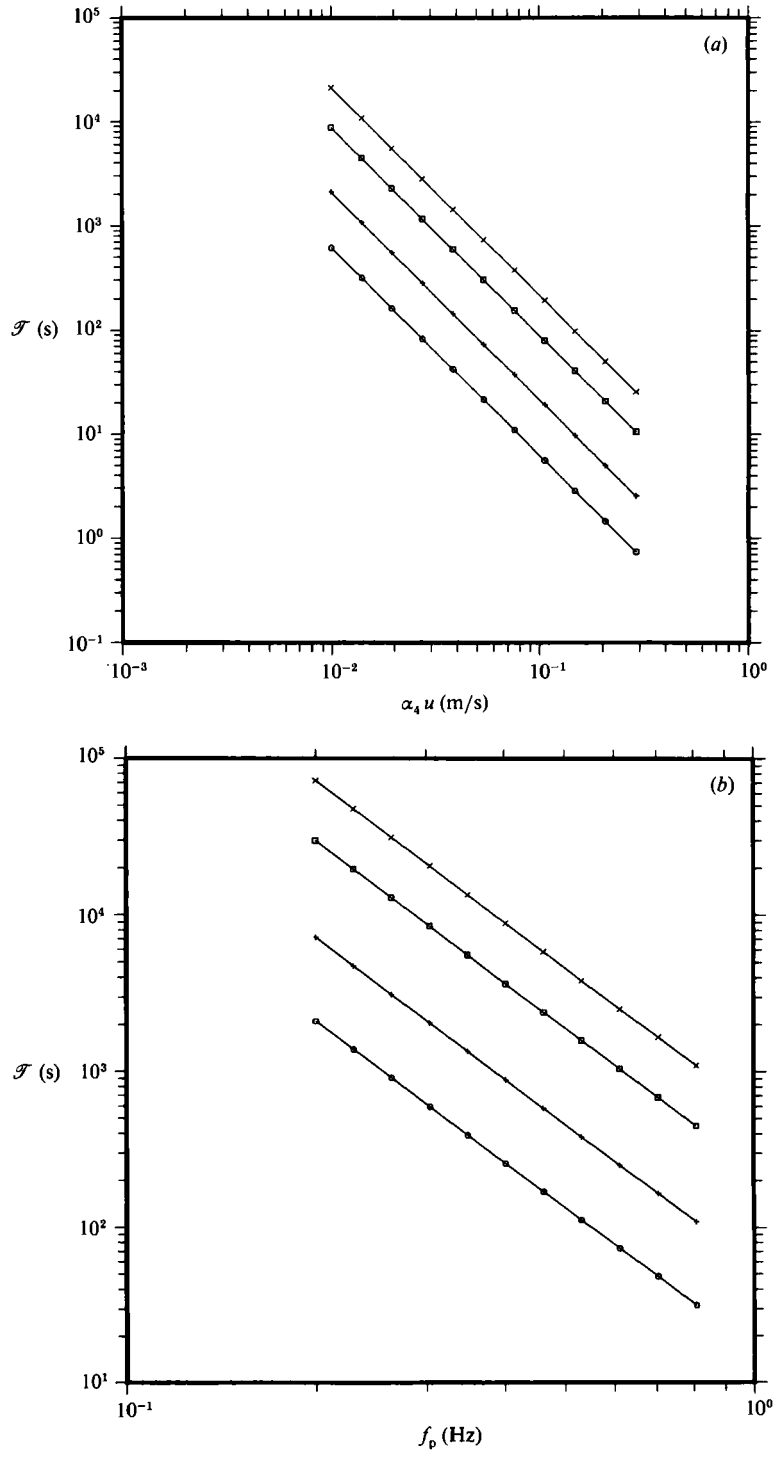

FIGURE 19. (*a*) Relaxation time defined by (5.3) as a function of $\alpha_4 u$: ○, $\gamma = 1$; +, $\gamma = 2$; □, $\gamma = 5$; ×, $\gamma = 10$. (*b*) As in (*a*) as a function of f_p.

nonlinear fluxes and is motivated by (3.5) relating the nonlinear transfer $\mathscr{S}_{\rm nl}$ to spectral fluxes.

To investigate the sensitivity of relaxation times defined by (5.3) with respect to peakedness γ, peak frequency $f_{\rm p}$ and $\alpha_4 u$, we combine (4.3), (4.12), and (5.3) and infer

$$\mathscr{T} = \frac{2g^2 f_{\rm p}^{-3}}{(\alpha_4 u)^2}, \tag{5.5}$$

where 2 is a non-dimensional constant depending on f_1, f_2 and spectral peakedness γ. Assuming an equilibrium range between $1.6f_{\rm p}$ and $2.5f_{\rm p}$, figure 19(*a*) shows the variation of $\mathscr{T}$ with $\alpha_4 u$ and γ, computed in the middle of the equilibrium range from (5.3). Similarly, figure 19(*b*) shows the variation of $\mathscr{T}$ with respect to $f_{\rm p}$ and γ. The agreement between (5.5) and figures 19(*a*) and 19(*b*) is remarkable. The exponents for $f_{\rm p}$ and $\alpha_4 u$ in (5.5) are obtained to 3 decimal places with correlation coefficients that are very near one. Relaxation times in these computations are seen to correspond to the results of the previous section. The mid-range abscissa in figure 19(*a*) is appropriate for wind speeds from 12 to 20 m s^{-1} with $f_{\rm p} = 0.3$.

6. Conclusions

A different perspective for nonlinear energy transfer due to wave–wave interactions in a spectrum has been suggested. Formulating an efficient numerical integration scheme for the nonlinear energy transfers first described by Hasselmann (1961), we calculated energy fluxes through the spectrum and the spectral evolution with time. The divergence of these fluxes is the conventional 'source term' formulation used in past parameterizations of nonlinear transfer due to wave–wave interactions. Moreover, fluxes appear to provide an important understanding of overall energy exchanges among various regions of the spectrum. We make the following conclusions:

(i) As described by Zakharov & Filonenko (1968), Kitaigorodskii (1983) and Resio (1987), and seen in figure 7, energy fluxes through the equilibrium range of a spectrum are approximately constant only for an f^{-4} spectrum, at frequencies sufficiently above the spectral peak.

(ii) Fluxes through a spectrum are independent of $f_{\rm p}$, as seen in figure 8; nonlinear energy transfers for an f^{-4} spectrum therefore scale as $\alpha^3 f_{\rm p}^{-1}$ rather than $\alpha^3 f_{\rm p}^{-4}$ as in the case of an f^{-5} spectrum.

(iii) Energy fluxes through the equilibrium range are independent of spectral peakedness and depend only on the local energy densities. This is evident in figure 9 and also the non-dimensional curves of figure 11. The lobes of the corresponding nonlinear energy transfers shift to higher frequencies with decreasing peakedness, particularly when peakedness is less than 1.0.

(iv) Decreasing peakedness while holding the energy of the peak constant leads to decreased sharpness, broader spectra, enhanced energy fluxes and nonlinear energy transfers. Concomitantly, the peaks of the lobes migrate to higher frequencies. This is shown in figures 12–14.

(v) Variations in peakedness produce more significant changes in energy fluxes than do variations in angular spreading. This compares figure 9 to figure 15. In either case, the range considered was taken to cover what could be expected to occur in nature.

(vi) The nonlinear energy transfer should be smooth, as shown in figure 3, even for very coarse integration grids. Section 5.2 demonstrated that wave–wave interactions

work to smooth perturbations introduced into the spectrum as spikes. The time taken for the nonlinear interactions to respond to any perturbation depends strongly on where it occurs within the spectrum.

(vii) Computations of relaxation time, expressed as the quotient of the equilibrium range energy by the sum of energy fluxes, agree well with equilibrium range flux parameterizations, as shown in figure 19. The more usual expression for relaxation time is the quotient of the equilibrium range energy by the nonlinear energy transfer $\mathscr{S}_{\mathrm{nl}}$.

We are motivated by these results to expect that it is possible to include the complete Boltzmann integral for nonlinear wave–wave interactions in a research wave model using the integration method of this paper. This approach should be an improvement over the present parameterizations of nonlinear transfer due to wave–wave interactions. Although the computer time required for this may still be prohibitive for operational wave modelling, it should be possible to investigate simple fetch- and duration-limited wave growth situations.

We want to thank Klaus Hasselmann for comments and criticisms over the past year and a half. These forced us to try to clarify our ideas and directed us in ways to improve our work.

We are thankful to Andrew McLeod who did much of the plotting under the supervision of Bechara Toulany; his work was supported by a Natural Sciences and Engineering Research Council Strategic Grant to John Walsh of the Centre for Cold Ocean Resource Engineering, Memorial University of Newfoundland.

This work was also supported by the Federal Panel on Energy Research and Development (PERD) of Canada.

REFERENCES

BARNETT, T. P. 1968 On the generation, dissipation, and prediction of wind waves. *J. Geophys. Res.* **73**, 513–529.

BARNETT, T. P. & SUTHERLAND, S. 1968 A note on an overshoot effect in wind-generated waves. *J. Geophys. Res.* **73**, 6879–6885.

DONELAN, M. A., HAMILTON, J. & HUI, W. H. 1985 Directional spectra of wind-generated waves. *Phil. Trans. R. Soc. Lond.* A **315**, 509–562.

EWING, J. A. 1971 A numerical wave prediction method for the North Atlantic Ocean. *Deutsche Hydrograph. Z.* **24**, 241–261.

FOX, M. J. H. 1976 On the nonlinear transfer of energy in the peak of a gravity-wave spectrum II. *Proc. R. Soc.* A **348**, 467–483.

HASSELMANN, D. E., DUNKEL, M. & EWING, J. A. 1980 Directional wave spectra observed during JONSWAP 1973. *J. Phys. Oceanogr.* **10**, 1264–1280.

HASSELMANN, K. 1961 On the nonlinear energy transfer in a gravity-wave spectrum. Part 1. General Theory. *J. Fluid Mech.* **12**, 481–500.

HASSELMANN, K. 1963*a* On the nonlinear energy transfer in a gravity-wave spectrum. Part 2. Conservation theorems; wave-particle analogy; irreversibility. *J. Fluid Mech.* **15**, 273–281.

HASSELMANN, K. 1963*b* On the nonlinear energy transfer in a gravity-wave spectrum. Part 3. Evaluation of the energy flux and swell-sea interaction for a Neumann spectrum. *J. Fluid Mech.* **15**, 385–398.

HASSELMANN, K., BARNETT, T. P., BOUWS, E., CARLSON, H., CARTWRIGHT, D. E., ENKE, K., EWING, J. A., GIENAPP, H., HASSELMANN, D. E., KRUSEMAN, P., MEERBURG, A., MÜLLER, P., OLBERS, D. J., RICHTER, K., SELL, W. & WALDEN, H. 1973 Measurements of wind–wave growth and swell decay during the Joint North Sea Wave Project (JONSWAP). *Deutsche Hydrograph. Z. Suppl. Ser.* A (8), no. 12.

HASSELMANN, K., ROSS, D. B., MÜLLER, P. & SELL, W. 1976 A parametric wave prediction model. *J. Phys. Oceanogr.* **6**, 200–228.

HASSELMANN, S. & HASSELMANN, K. 1981 A symmetrical method of computing the nonlinear transfer in a gravity-wave spectrum. *Hamburger Geophys. Einzelschr.* A **52**, 163 pp.

HASSELMANN, S. & HASSELMANN, K. 1985 Computation and parameterizations of the nonlinear energy transfer in a gravity wave spectrum. Part I: A new method for efficient computations of the exact nonlinear transfer integral. *J. Phys. Oceanogr.* **15**, 1369–1377.

HASSELMANN, S., HASSELMANN, K., ALLENDER, J. H. & BARNETT, T. P. 1985 Computation and parameterizations of the nonlinear energy transfer in a gravity wave spectrum. Part II: Parameterizations of the nonlinear energy transfer for application in wave models. *J. Phys. Oceanogr.* **15**, 1378–1391.

HASSELMANN, S., HASSELMANN, K., KOMEN, G. K., JANSSEN, P., EWING, J. A. & CARDONE, V. 1989 The WAM model – A third generation ocean wave prediction model. *J. Phys. Oceanogr.* **18**, 1775–1810.

KITAIGORODSKII, S. A. 1983 On the theory of the equilibrium range in the spectrum of wind-generated gravity waves. *J. Phys. Oceanogr.* **13**, 816–827.

KOMEN, G. J., HASSELMANN, S. & HASSELMANN, K. 1984 On the existence of a fully developed windsea spectrum. *J. Phys. Oceanogr.* **14**, 1271–1285.

LONGUET-HIGGINS, M. S. 1976 On the nonlinear transfer of energy in the peak of a gravity-wave spectrum: a simplified model. *Proc. R. Soc.* A **347**, 311–328.

MASADA, A. 1980 Nonlinear energy transfer between wind waves. *J. Phys. Oceanogr.* **15**, 1369–1377.

MITSUYASU, H., TASAI, F., SUHARA, T., MIZUNO, S., OHKUSO, M., HONDA, T. & RIKIISHI, K. 1975 Observations of the directional spectra of ocean waves using a cloverleaf buoy. *J. Phys. Oceanogr.* **5**, 750–760.

PHILLIPS, O. M. 1985 Spectral and statistical properties of the equilibrium range in wind-generated gravity waves. *J. Fluid Mech.* **156**, 505–531.

RESIO, D. T. 1981 The estimation of a wind–wave spectrum in a discrete spectral model. *J. Phys. Oceanogr.* **11**, 510–525.

RESIO, D. T. 1987 Shallow-water waves. I: theory. *J. Waterway Port, Ocean Engng* **113** (3), 264–281.

RESIO, D. T. & PERRIE, W. A. 1989 Implications of an f^{-4} equilibrium range for wind-generated waves. *J. Phys. Oceanogr.* **19**, 193–204.

SELL, W. & HASSELMANN, K. 1972 Computations of nonlinear energy transfer for JONSWAP and empirical wind-wave spectra. *Rep. Inst. Geophys.* University of Hamburg.

TOBA, Y., OKADA, K. & JONES, I. S. F. 1988 The response of wind–wave spectra to changing winds. Part I: Increasing winds. *J. Phys. Oceanogr.* **18**, 1231–1240.

TRACY, B. A. & RESIO, D. T. 1982 Theory and calculations of the nonlinear energy transfer between sea waves in deep water. *WES Rep.* 11, US Army Engineer Waterways Experiment Station, Vicksburg, MS.

WEBB, D. J. 1978 Nonlinear transfer between sea waves. *Deep-Sea Res.* **25**, 279–298.

ZAKHAROV, V. E. & FILONENKO, N. N. 1966 Energy spectrum for stochastic oscillations of the surface of a liquid. *Dokl. Akad. Nauk SSSR* **160** (6), 1292–1295.